Acta Pharmaceutica Sinica B 2026;16(4):2553−2569

Chinese Pharmaceutical Association
Institute of Materia Medica, Chinese Academy of Medical Sciences

Acta Pharmaceutica Sinica B

www.elsevier.com/locate/apsb
www.sciencedirect.com

ORIGINAL ARTICLE

Deep eutectic solvents@enteric technology for orally delivering anticoagulant macromolecule drug

Xiaoke He[a,†], Jiahui Zou[a,†], Yuxin Jiang[a,†], Runrui Liao[a], Huiling Liao[a], Yaping Liu[a], Yueming Zhao[b,*], Jing Yu[c,*], Wei He[d,*]

[a]*Department of Pharmaceutics, School of Pharmacy, China Pharmaceutical University, Nanjing 211198, China*
[b]*Department of Respiratory and Critical Medicine, Nanjing First Hospital, Nanjing Medical University, Nanjing 210000, China*
[c]*Department of Clinical Pharmacy, The First Hospital of Hebei Medical University, Shijiazhuang 050000, China*
[d]*Shanghai Skin Disease Hospital, Tongji University School of Medicine, Shanghai 200443, China*

Received 6 June 2025; received in revised form 26 August 2025; accepted 4 September 2025

KEY WORDS

Low molecular weight heparin;
Deep eutectic solvents;
Venous thromboembolism;
Absorption enhancers;
Enteric capsule;
Oral administration;
Macromolecule drug;
Anticoagulant

Abstract Low-molecular-weight heparin (LMWH) is one of the most clinically used anticoagulants to improve venous circulation. However, LMWH requires repeated injections, leading to poor medication compliance. Herein, we developed a deep eutectic solvents (DESs)@enteric technology, an intestinal absorption promotion platform, for the oral administration of LMWH. DESs with geranic acid (Ge) and choline (Ch) were first synthesized and characterized. Then, the DES−LMWH complex was prepared with a $DES_{2:1}$ (Ge and Ch in a 2:1 molar ratio), demonstrating superior intestinal absorption and high biocompatibility. Finally, DES−LMWH was granulated and loaded into an enteric capsule. *In vitro,* DESs reversibly opened the tight junctions between intestinal epithelial cells, facilitating the paracellular transport of LMWH. *In vivo*, the DES−LMWH oral enteric capsule demonstrated an absolute bioavailability of 19.93%, reaching the venous thromboembolism (VTE) prophylaxis threshold and reducing the embolization area by 52.01% in a $FeCl_3$-induced rat femoral venous thrombosis model. In conclusion, DES@enteric technology effectively enhances the oral absorption of LMWH and holds promising translational potential.

*Corresponding authors.
E-mail addresses: sabrina-zym@163.com (Yueming Zhao), yujing@hebmu.edu.cn (Jing Yu), weihe@cpu.edu.cn (Wei He).
[†]These authors made equal contributions to this work.

Peer review under the responsibility of Chinese Pharmaceutical Association and Institute of Materia Medica, Chinese Academy of Medical Sciences.

https://doi.org/10.1016/j.apsb.2025.10.037

1. Introduction

VTE is the third most common cardiovascular disease in the world after heart disease and stroke[1]. The annual incidence of VTE is 1‰−2‰ and is increasing year by year, plaguing nearly 10 million people globally[2,3]. Functional disturbance of vascular endothelial cells and blood coagulation abnormalities often induce a prothrombotic state (PTS)[4]. The factors, such as prolonged bed rest, surgery, pregnancy, cancer, obesity and advanced age, risk PTS and VTE, requiring anticoagulation therapy[5,6].

LMWH is widely used in anticoagulation therapy, prophylaxis and the treatment of VTE[7,8]. As an indirect thrombin inhibitor, LMWH comprises highly water-soluble polysaccharides derived from the chemical or enzymatic depolymerization of unfractionated heparin, with a molecular weight range of 3000−8000 Da. LMWH exhibits substantial negative charges in aqueous solution and associates with cations while maintaining chemical stability at approximately neutral pH (pH ∼7). Its anticoagulant mechanism of LMWH primarily involves catalyzing the inactivation of coagulation factor Xa and inhibiting the coagulation cascade reaction ultimately[9]. Compared to conventional oral anticoagulants (such as warfarin) or direct oral anticoagulants, LMWH demonstrates distinct clinical advantages: (i) a reduced drug−drug interaction profile, minimizing therapeutic conflicts in polypharmacy patients; (ii) minimal interference with platelet function, enabling more controllable bleeding risk management; (iii) non-transplacental passage, solidifying its status as the first-line anticoagulant during pregnancy[10-12]. However, due to its high molecular weight, substantial negative charges, susceptibility to enzymatic degradation, and instability in acidic environments, its oral bioavailability is significantly limited. As a result, LMWH requires parenteral administration, typically *via* subcutaneous injection[13]. For chronic anticoagulation therapy, frequent injections cause patient discomfort, local complications, infection and poor compliance. Therefore, oral preparation of LMWH is highly desired to improve patients' medication adherence.

Considering that the acidic gastric environment compromises the stability of most macromolecular drugs, the intestine represents a viable site for absorption. Enhancing intestinal permeability offers a reliable strategy to improve the oral bioavailability of LMWH[14]. Three primary approaches were reported to improve the intestinal LMWH absorption, including (i) prodrug formation through conjugation with lipid moieties to increase lipophilicity, (ii) ligand-mediated targeting *via* coupling LMWH or drug carriers to specific ligands, and (iii) formulating absorption enhancers (such as surfactants, chitosan and their derivatives, etc.)[15]. As the first two strategies often involve organic solvents and risk structural alteration of LMWH during synthesis[16]. The use of absorption enhancers provides a greener method with simpler preparation to improve the oral absorption of drugs[17]. This absorption enhancer has demonstrated efficacy in several macromolecular drug delivery systems. For example, Subedi et al.[18] used an alkyl glucoside-based non-ionic surfactant to formulate teriparatide, demonstrating a 13-fold increase in oral bioavailability compared to free teriparatide. While Xiao et al.[19] encapsulated peptides in milk exosome−liposome hybrid vesicles to overcome intestinal mucus and intracellular transport barriers. For LMWH specifically, Motlekar et al.[20] demonstrated the permeation-enhancing effect of L-arginine on a Caco-2 monolayer model. At a 2% concentration, L-arginine enhanced the *in vitro* permeability of LMWH 3-fold compared to controls. Besides, chitosan and its derivatives can activate tight junctions in epithelial cells, enhancing the paracellular transport of drugs[21,22]. Chitosan is typically prepared in the form of nanoparticles or microparticles for oral delivery of LMWH[21-23]. Bagre et al.[24] developed alginate-coated chitosan core−shell nanoparticles for the oral delivery of LMWH, increasing its oral bioavailability and the AUC by approximately threefold. However, these strategies are mostly cation-dependent and suffer from various demerits, including intense intestinal mucosal irritation, limited bioavailability improvements, complex manufacturing processes for nanoparticles and scalability challenges[25,26]. Accordingly, a new oral absorption enhancer is needed to enable the clinically viable delivery of oral LMWH.

Deep eutectic solvents (DESs) are liquid mixtures of anions (hydrogen bond donors) and cations (hydrogen bond acceptors) formed under certain conditions[27-29]. As a "green alternative" to organic solvents, DESs have the highlights of a simple preparation process, low volatility, high stability and non-flammability[30,31]. In addition, by changing the types and ratios of anions and cations, the physicochemical properties and biological activities of DESs can be altered[32]. Studies have shown that DESs with choline (Ch) as the hydrogen bond receptor have good biocompatibility[33]. Among the DESs formed by Ch and different hydrogen bond donors, DESs synthesized from Ch and geranic acid (Ge) may be a powerful absorption enhancer, as they exhibit excellent drug solubilization properties and significantly improve the intestinal permeability of the drug[34-36]. Banerjee et al.[37] demonstrated that DESs formed by Ch and Ge protected insulin from intestinal digestive enzymes, resulting in the thinning of the mucus layer and facilitating paracellular transport of insulin.

In this study, an oral formulation of LMWH based on DESs@enteric technology was developed to enhance oral bioavailability and facilitate the prevention of VTE. The Ch-Ge-based DESs were first synthesized and mixed with LMWH. DES−LMWH was loaded in oral enteric capsules to prevent the degradation of LMWH in acidic gastric juice. The optimal proportion and dosage of DESs were screened by the solubility of LMWH and the effect of intestinal absorption. The storage stability, pharmacokinetics, antithrombotic effect and safety were then evaluated using a combination of *in vitro* and *in vivo* tests. Additionally, the intestinal pro-absorptive effects of DES on LMWH and its mechanism of action were investigated. We demonstrated that the DES−LMWH oral enteric capsules released LMWH in the intestine, opened tight junctions between intestinal epithelial cells and reached the prophylactic dose of VTE. This study offers an emerging strategy for the oral delivery of LMWH. The preparation could be easily manufactured and safely controlled, which may improve medication compliance in VTE high-risk patients and have promising application prospects.

2. Materials and methods

2.1. Materials

Ge (85% solution) and Ch (80% solution) were purchased from Sigma−Aldrich (St. Louis, MO, USA). LMWH (110 IU/mg), Azure II and fluorescein sodium (analytical reagent) were purchased from Shanghai Macklin Biochemical Co., Ltd. (Shanghai, China). Enteric capsules were purchased from Shanghai Yuyan Instruments Co., Ltd. (Shanghai, China). Transwell polycarbonate membrane chambers were purchased from Nanjing Yuanzhixin Biotechnology Co., Ltd. (Nanjing, China). Dulbecco's modified Eagle's medium (DMEM) was purchased from Wuhan Servicebio Technology Co., Ltd. (Wuhan, China). FITC-Dextran 4000 (FD4), Chlorpromazine (CPZ), Methyl-β-Cyclodextrin (M-β-CD) and Amiloride (AMLR) were purchased from Shanghai Aladdin Reagent Co., Ltd. (Shanghai, China). Krebs-Ringer buffer was purchased from Beijing Solarbio Science & Technology Co., Ltd. (Beijing, China). 4,6′-diamidino-2-phenylindole (DAPI) was purchased from Shanghai Beyotime Biotechnology Co., Ltd. (Shanghai, China). 4% paraformaldehyde was purchased from Nanjing Chemical Reagent Co., Ltd. (Nanjing, China). The coagulation factor IXa activity assay kit (fluorometric) was purchased from Shanghai Boatman Biotech Co., Ltd. (Shanghai, China). An activated partial thromboplastin time (APTT) assay kit (coagulation) was purchased from Shanghai Yuanye Bio-Technology Co., Ltd. (Shanghai, China).

2.2. Animals

Sprague−Dawley rats (6−8 weeks, male, 250−300 g) were purchased from Qinglong Mountain Animal Breeding Ground (Nanjing, China). All animal experiments were conducted in accordance with the guiding principles of international animal experimentation, as outlined in the Experimental Animal Management Regulations and the Guiding Opinions on the Treatment of Experimental Animals. All animal protocols were approved by the China Pharmaceutical University Animal Care and Use Committee (No. 2022-10-011).

2.3. Preparations

DESs were prepared as previously reported[38]. DESs with Ge to Ch molar ratios of 4:1, 2:1, 1:1 and 2:3 were synthesized *via* a salt metathesis reaction. Briefly, an appropriate amount of Ch was mixed with Ge drop by drop, stirred at 40 °C until CO_2 production ceases, followed by rotary evaporation at 60 °C for 2 h and drying in a vacuum oven at 60 °C for 48 h. Next, DES−LMWH was prepared by mixing DESs with distilled water, adding LMWH and vortexing for 5 min. Finally, DES−LMWH was used as an adhesive, mixed with a specific amount of filler, and sieved through a 20-mesh sieve for granulation. This was followed by drying at 60 °C for 3 h and loading the particles into enteric capsules.

The optimized DES−LMWH oral enteric capsules were prepared in a similar process. The $DES_{2:1}$ was diluted with water to obtain 300 μL of 25% (*v*/*v*) $DES_{2:1}$, followed by mixing with 20 mg of LMWH, vortexing, mixing with 500 mg of mannitol, and sieving for granulation. The resulting granules were then dried and loaded into an enteric capsule.

2.4. Characterization of DESs

The synthesized DESs were placed in nuclear magnetic resonance (NMR) tubes containing coaxial inserts of dimethyl sulfoxide-d_6 (DMSO-d_6) and characterized using a Bruker Avance AV-300 MHz spectrometer (Bruker Corporation, Billerica, Massachusetts, USA). The Bruker Vertex 70v Fourier transform infrared spectrometer (FTIR, Bruker Corporation, Billerica, MA, USA) was used to scan the spectrum of the synthesized DESs. FTIR scans were performed in the range of 4000−450 cm^{-1} at 25 °C with a resolution of 1.0 cm^{-1}.

2.5. Stability studies

To investigate the stability of DES−LMWH in intestinal digestive fluid, a 0.5 mL sample was added to 9.5 mL of artificially simulated intestinal digestive fluid (pH 6.8 PBS containing 1% trypsin and 0.3% bile salts) at 37 °C, 100 rpm (SHA-C water bath shaker, Jiangsu Jincheng Instruments Co., Ltd., Changzhou, China). Samples were taken at specific time intervals, incubated at 70 °C to inactivate the enzyme, cooled, and then frozen. The supernatant was obtained by centrifugation. The LMWH activity was determined by the azure II method. To investigate the storage stability, freshly prepared DES−LMWH was stored at 4 and 25 °C. The content of LMWH was detected on Days 0, 1, 4, 7 and 14.

To assess the stability of DES−LMWH oral enteric capsules, three independent stability tests were conducted: (i) For the influencing factor test: DES−LMWH oral enteric capsules were placed under high temperature (60 °C), high humidity (25 °C, 90 ± 5% RH) and strong light (4500 ± 1500 Lx), samples were taken on the 0 and 10th day of followed by LMWH determination and capsule characterization; (ii) For the accelerated test: three prepared DES−LMWH oral enteric capsules were stored at 40 ± 2 °C, 75 ± 5% RH, samples were taken at 0, 1, 3 and 6 months. Then, the content of LMWH, capsule characteristics and *in vitro* release behavior at each time point was determined; (iii) For the long-term test: three prepared DES−LMWH oral enteric capsules were stored at 25 ± 2 °C, 60 ± 10% RH, samples were taken at month 0, 1, 3, 6 and 12, the drug content capsule characteristics and release were measured.

2.6. Paracellular pathway transport studies

The Caco-2 monolayer cell model was first prepared. Caco-2 cells were seeded at a density of 2×10^4 cells per well in Transwell polyester membrane 24-well plates. In brief, 0.4 and 0.6 mL of complete culture medium were added to the chamber and base well plate, followed by cultivation in an incubator, replacing culture medium at 24 h after inoculation, changing the medium every 2 days for the first 7 days and replacing the medium every day until 21 days for use. The transepithelial cell resistance values were measured on Days 1, 5, 10, 15, and 20 after culture.

The tightness of the Caco-2 monolayer cell model was assessed by determining transepithelial electrical resistance (TEER) using the Millipore Millicell ERS-2 epithelial voltohmmeter (Merck KGaA, Darmstadt, Germany)[39,40]. Place the ohmmeter in the clean bench for 30 min of UV sterilization, and use electrode 0 to zero it. Replace with electrode 1 to measure the resistance value of each well, with the long side of the electrode in contact with the bottom of the well plate and the short side tightly attached to the inner wall of the chamber. Measure each well three times. Set a blank chamber (uncultured cells) as the control group,

with the resistance value being the blank resistance value. When the TEER value exceeded 300 Ω cm^2, transport studies were conducted. The TEER value is calculated according to Eq. (1):

$$\text{TEER}\left(\Omega\cdot\text{cm}^2\right)=(R\text{t}-R_0)\times S \quad (1)$$

R_t and R_0 are the cell monolayer resistance measurements (Ω) and empty dish resistance measurements (Ω), respectively. S is the monolayer membrane area (cm^2).

Additionally, apparent permeability coefficient (P_{app}) values are necessary to evaluate the integrity of the Caco-2 monolayer cell model. The fluorescence values of the samples at 490 nm were determined using a Cytation 5 multi-mode microplate detection and cell imaging system (BioTek, Winooski, Vermont, USA), and the apparent permeability coefficient (P_{app}) of fluorescein sodium was calculated according to Eq. (2):

$$P_{app}=\frac{\text{dQ(t)}}{\text{dt}}\times\frac{1}{AC_0} \quad (2)$$

Q(t) is the total amount of drug transferred across the membrane from the compartment to the well plate (μg). A is the membrane area of the compartment (cm^2). C_0 is the initial concentration of the drug in the compartment (μg/mL).

Free LMWH and DES−LMWH were diluted using DMEM medium to prepare an aqueous solution with a concentration of 2.5 mg/mL LMWH. Then, 200 and 800 μL of DMEM medium were added to the Transwell chambers and well plates, respectively, followed by 30-min incubation, removing the medium in the chambers, adding 200 μL of LMWH and DES−LMWH samples, collecting a 100-μL sample from the well plate at various time points and adding an equal amount of fresh DMEM medium. The absorbance values of the samples were determined by the azure II method to calculate the amount of LMWH transported.

2.7. TEER measurement of DESs treated Caco-2 monolayer transwells

In brief, 200 and 800 μL of DMEM medium were added to the Transwell chambers and well plates, respectively, followed by 30-min incubation and TEER determination. Then, the chamber medium was replaced using DMEM containing 0.0, 0.5, 1.0 or 2.0 mg/mL DESs. The TEER values were determined at 1, 2, 3, 4 and 5 h after incubation. Finally, the chamber was filled with DMEM medium, and the TEER was measured 24 h after incubation.

2.8. Transcellular pathway transport studies

DMEM medium (200 μL) containing different cellular uptake inhibitors CPZ (10 μg/mL), M-β-CD (2.5 mmol/L), and AMLR (13 μg/mL), was added to the Transwell chambers. DMEM medium (600 μL) was added to the well plates. After incubation for 30 min, 200 μL of DES−LMWH was added and incubated for an additional 3 h. The amount of LMWH transport was calculated by taking 100 μL of the solution and measuring the absorbance value of the sample by the Azure II method.

2.9. Single-pass intestinal perfusion experiment

Rats were anesthetized and randomly divided into five groups: control group, $DES_{2:3}$ (Ge and Ch in a 2:3 ratio) group, $DES_{1:1}$ (Ge and Ch in a 1:1 ratio) group, $DES_{2:1}$ (Ge and Ch in a 2:1 ratio) group and $DES_{4:1}$ (Ge and Ch in a 4:1 ratio) group. The abdominal cavity of the rats was opened 3−4 cm along the ventral white line, and the jejunal segment was selected 15−25 cm below the pylorus. The jejunal segment was cannulated at both ends and connected to the peristaltic pump (Baoding Longer Precision Pump Co., Ltd., Baoding, China). The abdominal wound was covered with absorbent cotton and the abdomen was irradiated with a surgical lamp for heat preservation during the irrigation process. The contents of the intestinal segments were first flushed with saline and equilibrated with Krebs−Ringer buffer. Then, the perfusate was replaced with the preparation. At the end of the perfusion, the cleaned intestinal segments were cut into multiple 1−2 cm segments and placed in 4% paraformaldehyde fixative for 24 h. Photographs were recorded using an DM-2500 upright fluorescence microscope (Leica Microsystems Wetzlar Co., Ltd., Wetzlar, Germany). The drug concentration before and after perfusion was determined using a fluorescence spectrophotometer, and the effective intestinal permeability coefficient (P_{eff}) and absorption rate constant (K_a) were calculated for each group of preparations. The P_{eff} and K_a were calculated according to Eqs. (3) and (4):

$$P_{eff}=\frac{-\text{Q}\times\ln\dfrac{C_{out}\times V_{out}}{C_{in}\times V_{in}}}{2\pi lr} \quad (3)$$

$$K_a=\frac{1-\dfrac{C_{out}\times V_{out}}{C_{in}\times V_{in}}}{\pi lr^2} \quad (4)$$

C_{in} and C_{out} are the mass concentrations of the intestinal inlet and outlet perfusate (mg/mL), V_{in} and V_{out} are the volumes of the corrected intestinal inlet and outlet perfusate (mL), l and r are the length (cm) and cross-sectional radius (cm) of the perfused intestinal segments, Q is the perfusion rate (mL/min).

2.10. Pharmacokinetics studies

To validate the clinical LMWH dosage, rats were unintentionally divided into two groups: subcutaneous injection of free LMWH group (5 mg/kg) and subcutaneous injection of free LMWH group (1 mg/kg). Blood samples were collected at various time points to determine the anti-FXa activity. The anti-FXa activity of LMWH in the sample plasma was determined using the microchromogenic substrate method[41,42]. The data were analyzed pharmacodynamically using PKSolve (version 2.0, China Pharmaceutical University, Nanjing, China).

For the intestinal absorption study of DES−LMWH, rats were randomly divided into four groups: intravenous injection of free LMWH group (40 mg/kg), intestinal injection of free LMWH group (40 mg/kg), intestinal injection of DES−LMWH group (20 mg/kg), and intestinal injection of DES−LMWH group (40 mg/kg).

For the pharmacokinetics study of DES−LMWH oral enteric capsules, rats were indiscriminately divided into two groups: a free LMWH control group (20 mg/kg) and a DES−LMWH oral capsule preparation group (20 mg/kg).

2.11. $FeCl_3$-induced rat femoral venous thrombosis model

The femoral venous thrombosis model was prepared based on previous reports[43,44]. The rats (220−260 g) were randomly divided into 5 groups: wild type (WT) group, model group, subcutaneous injection of LMWH group (1 mg/kg), free-LMWH oral

enteric capsule group (20 mg/kg) and DES−LMWH oral enteric capsule group (20 mg/kg). Continuous drug administration was performed for 7 days. The rats were anesthetized 1 h after the final administration, dissected, and the left femoral vein was used. Thrombus formation was induced by placing a filter paper (4 mm × 10 mm) soaked in 10% $FeCl_3$ on the left femoral vein for 5 min.

At 1 h after administration, blood was collected into tubes containing 0.109 mol/L trisodium citrate for subsequent coagulation parameter measurements (anticoagulant: blood = 1:9, *v*/*v*), including prothrombin time (PT), activated partial thromboplastin time (APTT), fibrinogen (FIB), and thrombin time (TT). The blood was centrifuged at 1000×*g* for 10 min at room temperature to obtain plasma. The four blood parameter assays were performed using the clotting time method[45,46]. Subsequently, the embolized femoral veins were collected for the measurements of thrombus length, wet weight and dry weight. Then, the embolized femoral veins were fixed in 4% paraformaldehyde for hematoxylin and eosin (H&E) staining and Masson staining.

2.12. Statistical analysis

Statistical results were presented as the mean ± standard deviation (SD) of at least three independent experiments. Experimental data were analyzed using GraphPad Prism (version 9.0; GraphPad Software, San Diego, CA, USA). $P < 0.05$ was regarded as statistically significant.

3. Results

3.1. Synthesis and characterization of DESs

First, DESs were synthesized by salt metathesis reaction. The structural formulas of Ge and Ch were shown in Fig. 1A. The appearances of DESs with different composition ratios are shown in Fig. 1B. As the proportion of Ch increased, the color of DESs darkened gradually, from yellow to orange-red.

Next, to validate the formation of DESs and the interactions between Ge and Ch, we employed experiments comprising ^{1}H nuclear magnetic resonance (NMR) and Fourier transform infrared spectroscopy (FT-IR) to characterize the structures of the DESs. As shown in Fig. 1C, the hydrogen atom groups belonging to Ge, Ch, and DESs, respectively, are observed in the ^{1}H NMR spectrum (Fig. 1C). After DES synthesis, the hydrogen atom groups in the Ch fragment had little chemical shift. While in the Ge fragment, the two terminal methyl groups (labeled 11 and 12) shifted from 2.58 to 1.31 ppm, followed by the changes (from 3.11 to 1.74 ppm) in internal methyl groups (labeled 5, 6, and 10). The protons (labeled 3 and 7) linked to the sp2 carbon shifted from 6.60 to 5.31 ppm and from 6.11 to 4.80 ppm, respectively. The data indicated that the synthesized DESs possessed the structure of both Ge and Ch. Notably, the single peak of carboxyl hydrogen in the Ge fragment located at 11.61 ppm disappeared, suggesting hydrogen bonds might form between carboxyl hydrogen in Ge and the nitrogen atom in Ch. Fig. 1D shows the ^{1}H NMR spectra of DESs with different composition ratios. Compared with Ge and Ch fragments, the hydrogen atom groups in the four DESs' hydrogen spectra all exhibited chemical shifts of varying degrees, further demonstrating the formation of DESs.

Then, the study of FTIR spectra confirmed the hydrogen bonds. As shown in Fig. 1E, the characteristic peaks of $DES_{2:1}$ were shifted towards the low wavenumber region compared to those of Ge and Ch. The peak of the C−OH stretching vibration shifted from 3232 to 3220 cm^{-1}, the peak of the Ge carbonyl stretching vibration shifted from 1686 to 1644 cm^{-1}, while the peak of the −C−O− stretching vibration shifted from 1247 to 1228 cm^{-1}. These changes indicated the formation of hydrogen bonds between Ge and Ch. Ch is a well-known hydrogen bonding receptor and readily forms hydrogen bonds with natural acids[47,48]. In addition, the intensity of the absorption peak of DESs at 3232 cm^{-1} gradually weakened and, while the intensity of the absorption peak at 1686 cm^{-1} gradually increased with the expansion of Ge ratio (Fig. 1F). The results of ^{1}H NMR and FT-IR confirmed the synthesis of DESs, while hydrogen bonds were the primary driver of DES formation.

3.2. Optimizing the formulation and characterization of DES−LMWH

DES−LMWH were prepared by the vortex method (Fig. 2A). We optimized the formulation by studying the DESs' ability to solubilize LMWH and their permeability-promoting effect. Studies have shown that the solubility of a solute in DESs is related to its polarity magnitude, with non-polar compounds being more soluble in pure DESs and highly polar compounds being more soluble in DESs containing water[49]. LMWH is a hydrophilic drug with a high polarity and an extremely low solubility of almost zero in pure DESs. The introduction of water could disintegrate part of the DESs' spatial structure, reduce viscosity, and solubilize other molecules. As an initial step, we established a method to determine LMWH using ultraviolet and visible (UV−Vis) spectrophotometry, employing azurite II as a cationic dye (Supporting Information Fig. S1 and Table S1)[50,51]. Fig. 2B showed the solubility of LMWH in different composition ratios and various concentrations of DESs. When the composition ratio of DESs was determined, the solubility of LMWH decreased with the increase in DES concentration. The maximum solubility of LMWH in DESs was only 277.12 mg/mL, possibly due to DESs still maintaining part of their spatial structure in water, and their high viscosity gave it less space to dissolve other solutes[52]. Additionally, when the concentration of DESs was the same, the higher the Ch content in the component, the higher the solubility of LMWH. This might be due to the high hydrophilicity and polarity of Ch. When the content of Ch was higher, the hydrophilicity of the formed DESs was stronger; thus, the solubilizing ability for hydrophilic LMWH increased.

To characterize the permeability-promoting effect of DESs, an *in vivo* intestinal perfusion model was established, as it retained the integrity of the intestinal vasculature and peripheral nerves in proximity to the intestinal environment, allowing for more accurate prediction of drug absorption behavior in the intestines[53,54]. FITC-Dextran 4000 (FD4), a FITC-labeled neutral dextran with an average molecular mass of approximately 4000 Da, has a chemical composition and molecular weight similar to those of LMWH. As a fluorescent tracer, FD4 emits bright fluorescence under specific excitation wavelengths, making it a widely adopted tool for studying intestinal permeability[55]. Given its high molecular weight, FD4 has a poor ability to traverse the intestinal epithelia under physiological conditions. Consequently, detecting the amount of FD4 transcellular transport directly reflects the magnitude of intestinal permeability. This property renders FD4 an effective benchmark for evaluating the permeability-enhancing efficacy of oral absorption enhancers in many reported studies[56-60]. Although FD4 and LMWH exhibit distinct charge profiles, FD4

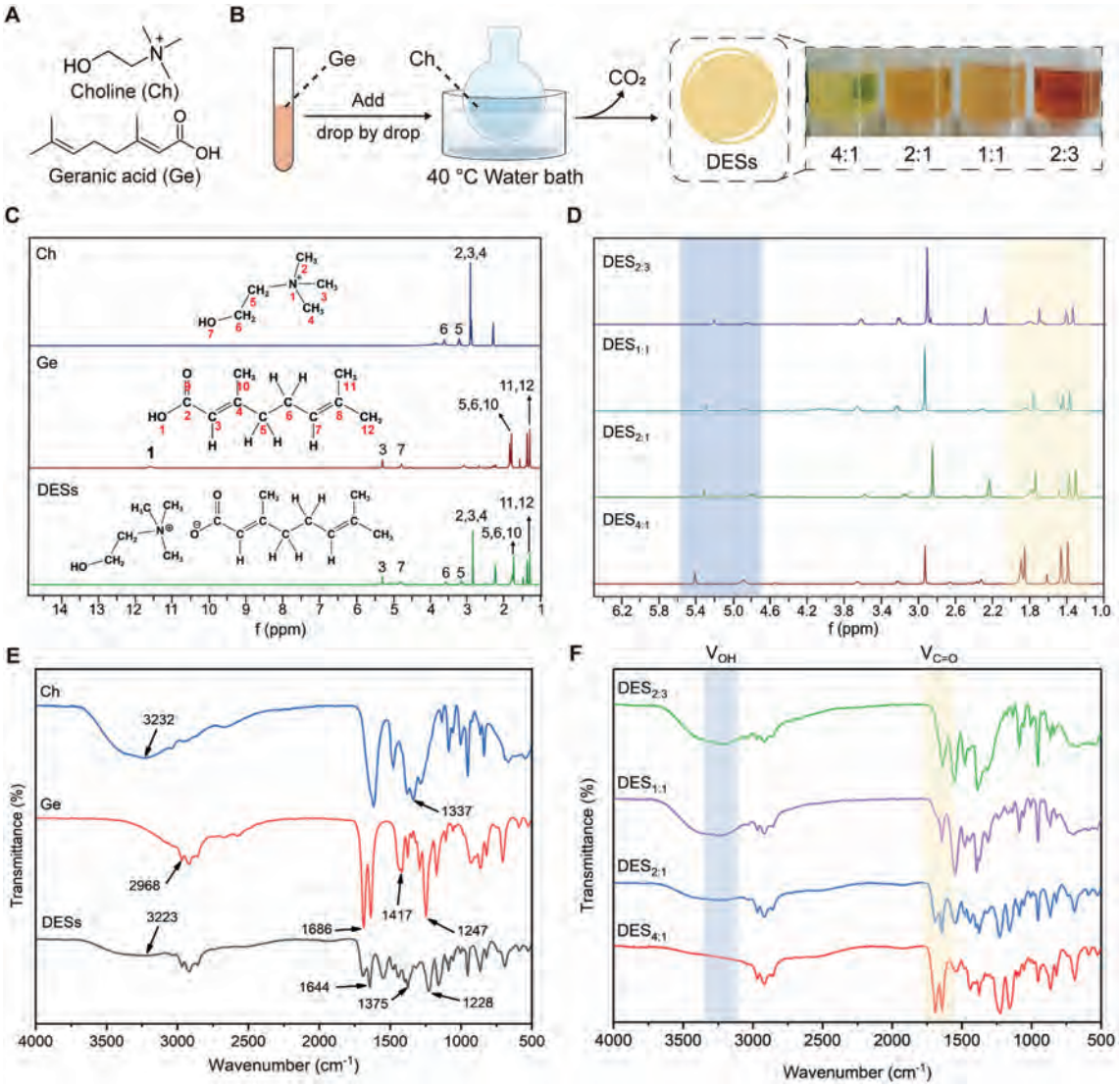

Figure 1 Synthesis and characterization of DESs. (A) Chemical structures of Ch and Ge. (B) DESs (Ge: Ch molar ratios of 4:1, 2:1, 1:1 and 2:3) were prepared by salt metathesis of Ge and Ch. (C) ^{1}H NMR spectra of Ch, Ge and DESs. (D) ^{1}H NMR spectra of $DES_{2:3}$, $DES_{1:1}$, $DES_{2:1}$ and $DES_{4:1}$. (E) FTIR spectra of Ch, Ge and DESs. (F) FTIR spectra of $DES_{2:3}$, $DES_{1:1}$, $DES_{2:1}$ and $DES_{4:1}$. FTIR scans were performed in the range of 4000−450 cm^{-1} at 25 °C with a resolution of 1.0 cm^{-1}.

permeability remains a valid screening indicator for selecting DES formulations with optimal intestinal permeability-enhancing capacity, owing to their molecular weight-dependent transport mechanisms. Therefore, FD4 was utilized as a model compound to study the LMWH intestine permeability. As shown in Fig. 2C and D, DESs with varying composition ratios enhanced the absorption of FD4 in the jejunum. $DES_{2:1}$ had the most significant pro-absorption effect, with a 3-fold P_{eff} and K_a compared to the free FD4 solution, and thereby was selected for the following study. Additionally, studies have shown that larger amounts of DESs may be more conducive to enhancing permeability[61]. Nevertheless, based on the solubility determination in the previous text, we demonstrated that the lower the concentration of DES_S, the more beneficial it was to the dissolution of LMWH. Considering the dosage requirements for subsequent experiments and the permeability-promoting effect, 25% DES was finally selected for the subsequent study.

To evaluate the contributions of structure to absorption enhancement, we characterized the physical state of 25% DESs and DESs−LMWH. First, they manifested as a uniform system (Supporting Information Fig. S2A and S2B). The 10-fold dilution using pH 6.8 PBS to simulate the state of drugs after dissolution in the intestinal environment allowed them to form colloidal formulation containing micelles or emulsions, demonstrating the diameter of 79.05 ± 3.58 nm (PDI 0.112 ± 0.013) and 196.60 ± 8.81 nm (PDI 0.292 ± 0.019), respectively (Fig. 2E and F). Transmission electron microscopy (TEM) examination revealed that the two diluted formulations had sub-spherical and relatively irregular rod-shaped structures with similar diameters, as determined by dynamic light scattering (DLS) analysis (Fig. 2G and H). The results confirmed the formation of colloid after dilution, and the growth of particle size and changes in morphology demonstrated the encapsulation of LMWH in the 25% DESs. DESs possess the hydrophobic heads of Ge and the hydrophilic tails of Ch. As a result, we speculated that DESs could self-assemble in the aqueous phase. As the drug-loaded DES is delivered to the intestine, it is diluted by intestinal fluid, forming a

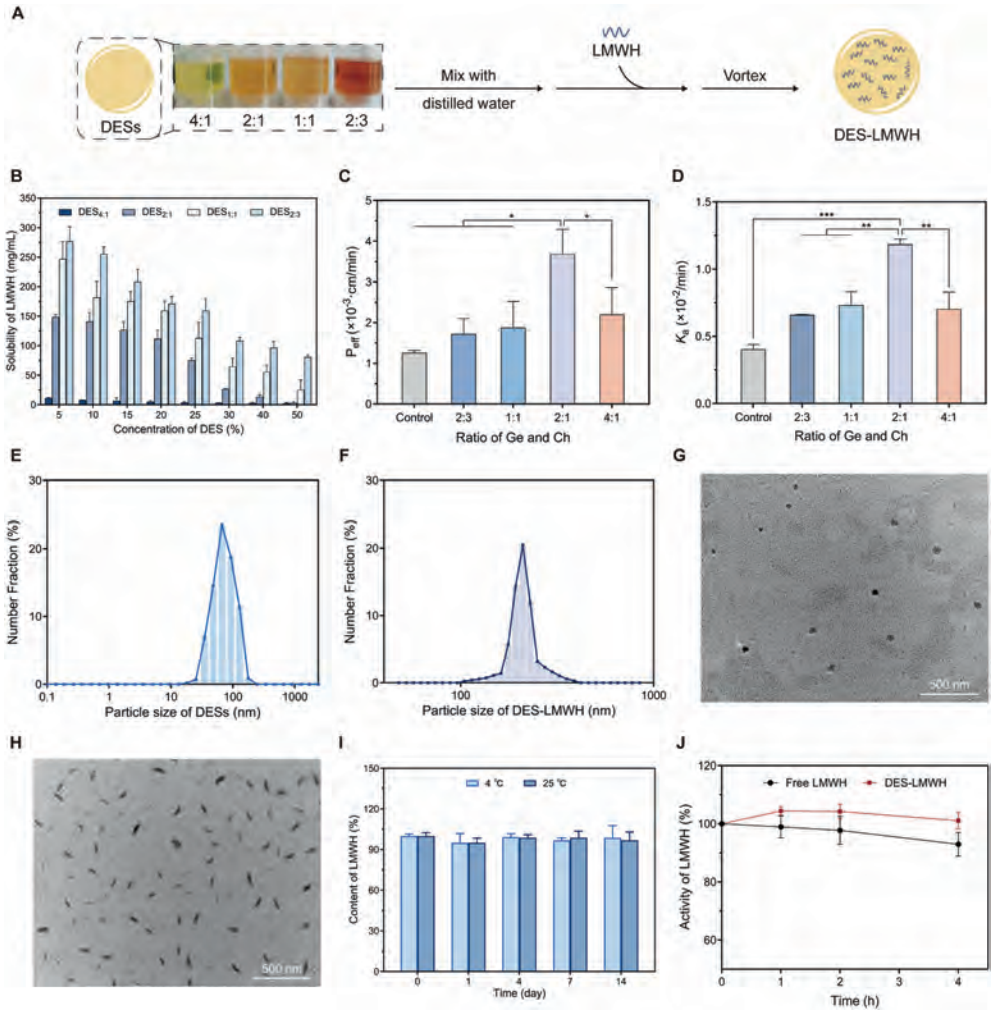

Figure 2 Optimizing the formulation and characterization of DES−LMWH. (A) DES−LMWH was prepared by the vortex method. (B) Solubility of LMWH in DESs with different concentrations and Ge: Ch molar ratios. (C, D) The effect of composition ratios of DES on the pro-absorption of FD4 in the jejunal segment was evaluated using *in vivo* intestinal perfusion in rats, with P_{eff} and K_a as indicators. Histograms of P_{eff} (C) and K_a (D) for each group of preparations in the intestinal perfusion experiment *in vivo*. $^*P < 0.05$, $^{**}P < 0.01$, $^{***}P < 0.001$, $^{****}P < 0.0001$ *vs.* 2:1 group. (E, F) Particle size of 25% DESs (E) and DES−LMWH diluted 10-fold using pH 6.8 PBS (F). (G, H) TEM of 25% DESs (G) and DES−LMWH, both diluted ten times with pH 6.8 PBS (H). Scale bar: 500 nm. (I) The stability of DES−LMWH under different storage conditions. (J) The activity of DES−LMWH in intestinal digestive juice. Data are presented as mean ± SD, $n = 3$.

micellar structure that may increase intestinal permeability through diffusion and fusion during drug delivery[35].

Finally, the storage and intestinal digestion stability of DES−LMWH were studied. The drug content remained unchanged after 14-day storage at 25 or 4 °C (Fig. 2I). Furthermore, DESs protected LMWH from digestion in intestinal fluid. As shown in Fig. 2J, the residual activity of free LMWH in simulated intestinal fluid decreased with prolonged digestion time to 92.97% after 4 h incubation. By contrast, drug activity in DES−LMWH remained around 100%. The results demonstrated good storage stability and enzymatic resistance properties of DES−LMWH.

3.3. Characterization of DES−LMWH oral enteric capsules

DES−LMWH oral enteric capsules were prepared by wet granulation (Fig. 3A), using mannitol as the filler of enteric capsules and DES−LMWH as the adhesive. To screen the prescription, we investigated the types of fillers and the dosage of adhesives. As demonstrated in Supporting Information Table S2, due to the strong hygroscopicity, the soft material made by sorbitol was too viscous to be granulated. At the same time, the content uniformity of capsules prepared with mannitol and lactose as fillers was 7.36% and 10.93%, respectively, meeting the standard requirement of the 2020 Chinese Pharmacopoeia (<15%). To avoid lactose intolerance caused by excipients, we selected mannitol as the filler. Then, the influence of adhesive dosage was examined. As shown in Supporting Information Table S3, when the amount of $DES_{2:1}$ was 250, 300, and 350 μL, the content uniformity of the capsules was 10.98%, 7.36%, and 10.93%, respectively, which conformed to the standards of the *Chinese Pharmacopoeia* (<15%). Thus, we chose 300 μL as the optimal adhesive dosage, for the content uniformity was minimized (7.36%), indicating a more uniform distribution of the drug in the capsules. The final DES−LMWH oral enteric capsules had a neat and smooth appearance, with no discernible odor. The drug content and moisture content were respectively 98.51% and 3.06%, with a

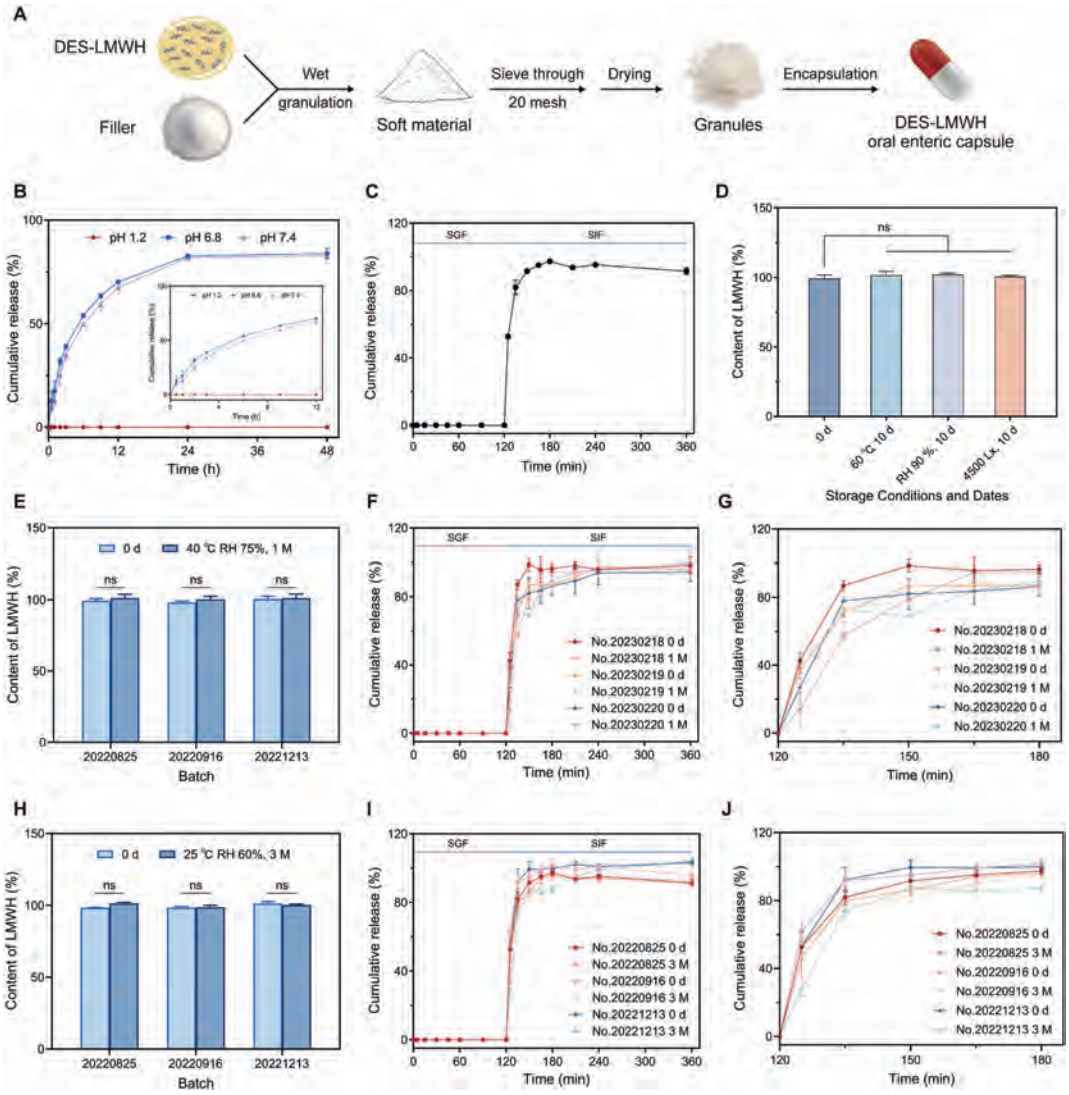

Figure 3 Release and stability of DES−LMWH oral enteric capsules. (A) DES−LMWH oral enteric capsules were prepared by the wet granulation technique. (B) *In vitro* release of DES−LMWH oral enteric capsule contents in PBS ($n = 5$). (C) Dissolution curve of DES−LMWH oral enteric capsules. SGF, simulated gastric juice; SIF, simulated intestinal juice. ($n = 5$). (D) Drug content after influencing factors test of DES−LMWH oral enteric capsules. (E) Drug content of accelerated test samples of DES−LMWH oral enteric capsules ($n = 3$). (F, G) Dissolution profiles (F) and dissolution profiles-120 to 180 min (G) of accelerated test samples of DES−LMWH oral enteric capsules ($n = 3$). (H) Drug content of long-term test samples of DES−LMWH oral enteric capsules ($n = 3$). (I, J) Dissolution profiles (I) and dissolution profiles-120 to 180 min (J) of long-term test samples of DES−LMWH oral enteric capsules ($n = 3$). Data are presented as mean ± SD. ns, not significant. d, day (s); M, month(s).

loading variance of 1.63% and a content uniformity of 7.36% (Supporting Information Table S4).

Next, we studied the *in vitro* release of DES−LMWH oral enteric capsules. To select the appropriate media for the *in vitro* release experiment, we first investigated the equilibrium solubility of LMWH in various release media, including distilled water, 0.1 mol/L HCl, pH 6.8 PBS, and pH 7.4 PBS. The solubility of LMWH in a non-acidic release medium was approximately 400 mg/mL, while in 0.1 mol/L HCL, it was 240.08 ± 9.46 mg/mL (Supporting Information Fig. S3A). The data indicated that these release media meet the sink condition of the determination requirement completely. Then, we tested the stability of LMWH in these release media. As depicted in Fig. S3B−S3F, LMWH maintained stability in distilled water, pH 6.8 PBS and pH 7.4 PBS and, in contrast, decreased by 15% in an acidic environment. DES−LMWH demonstrated similar pH-related stability (Fig. 3B). DES−LMWH released more than 80% of LMWH within 48 h in pH 7.4 and pH 6.8 PBS, while little LMWH was detected in pH 1.2 conditions. The results indicated that LMWH was stable in physiological and intestinal fluid environments, but unstable in simulated gastric environments, highlighting the necessity of an enteric-release design. As shown in Fig. 3C, the DES−LMWH oral enteric capsules released little LMWH in gastric fluid at 2 h and 96.38% in intestinal fluid at 180 min (Fig. 3C), meeting the standards of the *2020 Chinese Pharmacopoeia*.

To illustrate the capsule stability, we stored the samples under high temperatures (60 °C), high humidity (25 °C, 90 ± 5% RH), and intense light (4500 ± 500 Lux) for 10 days. As shown in

Supporting Information Table S5, the appearance of DES−LMWH oral enteric capsules remained intact and smooth without cracks after 10-day storage. The LMWH content remained 90%−110% of the initial value (Fig. 3D). Mass variation analysis revealed weight losses of 3.48% and 1.58% under high temperature and intense light, respectively, while high humidity induced a 1.54% mass gain (Table S5), which were all in accordance with the provisions of the *Chinese Pharmacopoeia* (<5%). Further accelerated (40 ± 2 °C, 75 ± 5% RH) and long-term (25 ± 2 °C, 60 ± 5% RH) test stability studies demonstrated consistent results: no macroscopic morphological changes were observed, and the weight changes remained below 5% (Supporting Information Tables S6 and S7). The LMWH content was maintained within 90%-110% throughout the testing periods (Fig. 3E and H). Notably, the *in vitro* release profiles of three production batches in the same test exhibited high consistency both before and after testing (Fig. 3F, G, I, and J). Overall, the stability studies demonstrated good storage stability and batch-to-batch reproducibility.

3.4. Clinical equivalence and bioavailability of oral enteric capsules

The pharmacokinetic profiles of the preparations were assessed in rats using mean plasma concentration−time curves, and the pharmacokinetic parameters were calculated using a non-compartmental model. Biological potency assays are adopted by the pharmacopeias of many countries for LMWH quality control; these methods measure anticoagulant activity *via* plasma clotting time or anti-Xa activity[62]. As they are precise and accurate, the assays are suited for complex *in vivo* matrices where sensitivity is critical. The plasma LMWH concentration was quantified using the anti-FXa micro chromogenic substrate method due to: (i) LMWH's preferential inhibition of factor Xa over IIa, (ii) superior accuracy for *in vivo* samples and (iii) direct correlation to pharmacological activity[41].

The pharmacokinetic study included three sections (Fig. 4A). Consistent with clinical guidelines for LMWH application in VTE, the ideal blood concentration range was defined as 0.1−0.5 IU/mL (prophylaxis) and 0.5−1.0 IU/mL (treatment)[63,64]. To validate the therapeutic and prophylactic anti-FXa activity of LMWH under clinical dosage, we compared the pharmacokinetic behavior of subcutaneous injection-free LMWH at 5 and 1 mg/kg as a contrast. As shown in Fig. 4B, subcutaneous administration at 5 mg/kg maintained a therapeutic concentration for 3 h and a prophylactic concentration for an additional 1 h, with a C_{max} of 1.61 IU/mL and an $AUC_{0-24\ h}$ of 3.33 IU·h/mL. In contrast, subcutaneous administration at 1 mg/kg demonstrated a 6-h-lasting duration of prophylactic effect.

Then, to explore the feasibility of LMWH intestinal delivery using DES and a clinical equivalent dose for subsequent capsule filling and administration, we evaluated the pharmacokinetics of intermediate preparations (DES−LMWH) following intestinal injection. As shown in Fig. 4C and D and Supporting Information Table S8, the LMWH plasma concentration and bioavailability from DES−LMWH significantly increased compared to free LMWH at equivalent doses. The absolute bioavailability of free LMWH is extremely low at 5.47%. In contrast, DES−LMWH exhibited substantially improved absorption, with a relative bioavailability of 331.79% and an absolute bioavailability of 18.16% (a 3.3-fold increase over the free drug). Statistical analysis revealed significant differences in both C_{max} ($P < 0.05$) and $AUC_{0-24\ h}$ ($P < 0.01$) between the free LMWH 40 mg/kg (i.j.) group and DES−LMWH 40 mg/kg (i.j.) group (Fig. 4E), confirming the DES's capacity to improve the bioavailability of LMWH. Additionally, the T_{max} of the DES−LMWH 40 mg/kg (i.j.) group was lower than that of the free LMWH 40 mg/kg (i.j.) group, indicating that DESs accelerated intestinal absorption. Intriguingly, the intestinal delivery of both 40 and 20 mg/kg DES−LMWH achieved comparable durations of therapeutic target (3 h) and prophylactic target (3−6 h), despite the 8- and 4-fold higher dose requirements. This dose−exposure relationship indicated that optimized oral preparations of DES−LMWH could achieve clinical equivalence to subcutaneous LMWH injections (5 mg/kg), providing evidence for advancing DES−LMWH as a viable oral anticoagulant.

Finally, we investigated the pharmacokinetics and clinical equivalence of enteric capsules following oral administration (Fig. 4F and G, and Table 1). It should be noted that due to limitations in capsule loading and the volume of rat administration, we were ultimately able to achieve a maximum dosage of 20 mg/kg. The capsules demonstrated a 189.66% relative bioavailability and an absolute bioavailability of 19.93%, representing a 1.9-fold enhancement over free LMWH (Fig. 4H). Moreover, compared to the subcutaneous administration of LMWH (1 mg/kg), the half-life of the DES−LMWH 20 mg/kg (*p.o.*) group increased from 2.62 to 6.14 h, resulting in a flatter plasma concentration level and reducing the risk of over-anticoagulation. However, compared to the DES−LMWH 20 mg/kg (i.v.) group, the DES−LMWH 20 mg/kg (*p.o.*) group achieved only the prophylactic target but failed to reach the therapeutic target. This may be due to drug loss during capsule preparation or the addition of excipients that limit the release rate of LMWH. Despite that, the DES−LMWH oral enteric capsules still demonstrated bioavailability enhancement and prolonged the action time, extending the duration of prophylactic target to over 8 h. Collectively, the 8-h lasting plasma concentration and the approximately 20% oral bioavailability indicate the promising clinical translation of the capsules. The capsule formulation might be an alternative for VTE prophylaxis, PTS management, and assisted reproduction technologies.

3.5. Mechanism of DESs promoting intestinal absorption of LMWH

We studied the transport of DES−LMWH in the Caco-2 monolayer cell model (Fig. 5A and Supporting Information Fig. S4). First, we evaluated the safety of DES through *in vitro* cytocompatibility assessments. Cell *via*bility remained above 90% after DES incubation at concentrations of 0.5−2.0 mg/mL (Fig. 5B), demonstrating negligible cytotoxicity. DESs improved the two cargoes, LMWH and FD4, to penetrate the monolayer in a concentration- and time-dependent manner (Supporting Information Fig. S5 and Fig. 5C). To investigate the penetration mechanism of DES, we determined the transepithelial electrical resistance (TEER) value in Caco-2 Transwells treated with varying concentrations of DESs (Fig. 5D). The 5-h incubation significantly reduced TEER while maximal drug translocation was achieved. The reduction rate was positively correlated with DES concentration. At the same time, the TEER in each group recovered to more than 95% of its original value after incubation in a DES-free medium for 24 h. The result indicated that DESs promoted the penetration across the Caco-2 monolayer by temporarily disrupting the tight junctions.

Then, we explored the transmembrane transport of DES−LMWH using pharmacological inhibitors to block the main

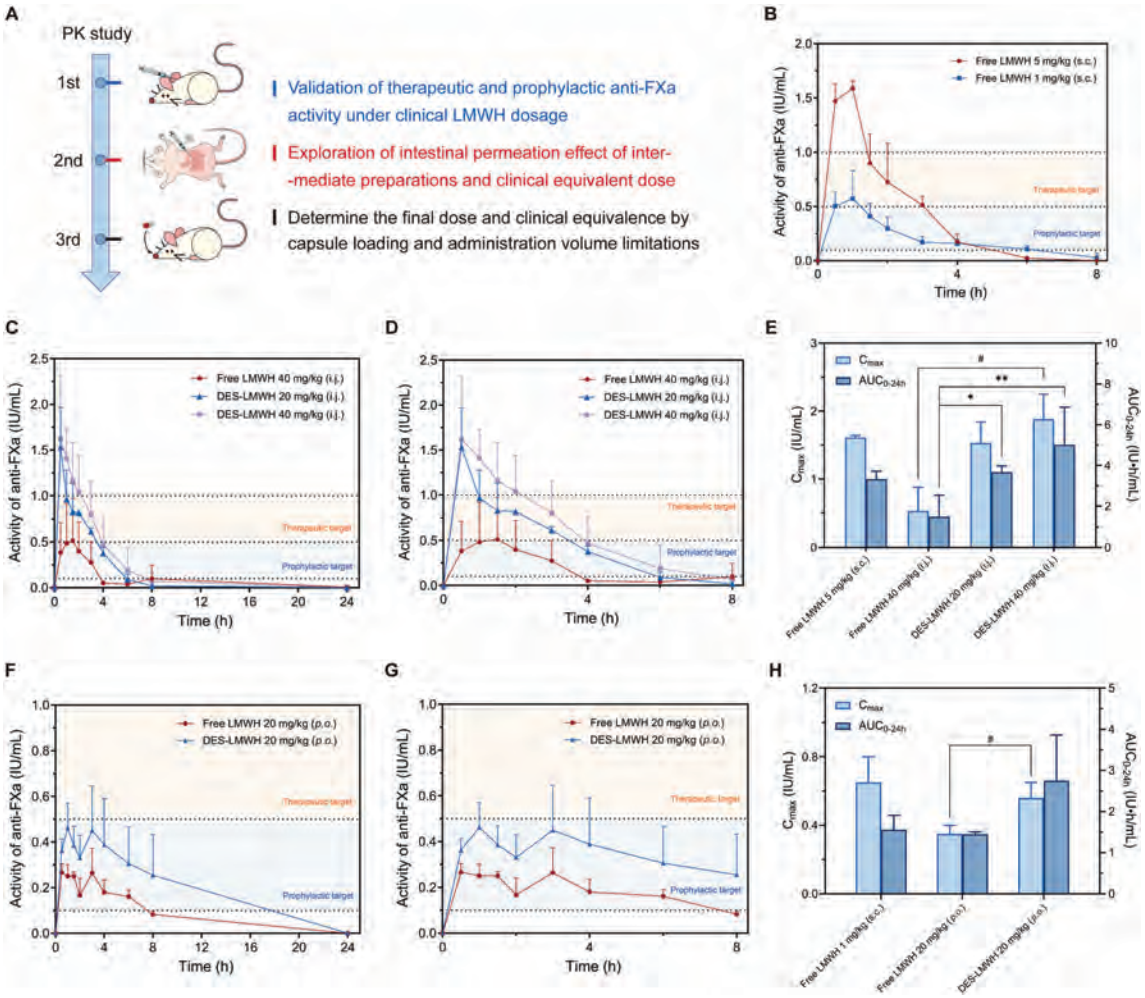

Figure 4 Pharmacokinetics and bioavailability of DES−LMWH and DES−LMWH oral enteric capsules. (A) The design basis of a pharmacokinetic study. (B) Drug concentration−time curve of clinical LMWH therapeutic and prophylactic dose after subcutaneous administration. (C−E) Drug concentration−time curve-24 h (C), drug concentration−time curve-8 h (D) and main pharmacokinetic parameters (E) of DES−LMWH after intestinal administration. $^{*}P < 0.05$, $^{**}P < 0.01$ *vs.* AUC_{0-24h} of Free LMWH 40 mg/kg (i.j.) group; $^{\#}P < 0.05$ *vs.* C_{max} of Free LMWH 40 mg/kg (i.j.) group. (F−H) Drug concentration−time curve-24 h (F) and drug concentration−time curve-8 h (G) and main pharmacokinetic parameters (H) of DES−LMWH oral enteric capsules. $^{\#}P < 0.05$ *vs.* C_{max} of Free LMWH 20 mg/kg (*p.o.*) group. Data are presented as mean ± SD, $n = 5$.

Table 1 Pharmacokinetic parameters of DES−LMWH oral enteric capsules ($n = 5$).

Materials	Dose (mg/kg)	$t_{1/2}$[a] (h)	T_{max}[b] (h)	C_{max}[c] (IU/mL)	$AUC_{0-24\ h}$[d] (IU·h/mL)	MRT[e] (h)
Free LMWH (i.v.)	40	1.41 ± 0.27	0.50 ± 0.00	11.11 ± 4.02	27.59 ± 8.82	2.06 ± 0.48
Free LMWH (s.c.)	1	2.62 ± 0.84	1.17 ± 0.24	0.65 ± 0.15	1.56 ± 0.35	3.99 ± 1.00
Free LMWH (*p.o.*)	20	3.54 ± 1.30	1.50 ± 1.08	0.35 ± 0.05	1.45 ± 0.06	5.87 ± 1.31
DES-LMWH[f] (*p.o.*)	20	6.14 ± 3.12	2.67 ± 1.25	0.56 ± 0.09[g]	2.75 ± 1.11	9.55 ± 4.79

Data are presented as mean ± SD, $n = 5$.

i.v., intravenous injection; s.c., subcutaneous injection; *p.o.*, per oral enteric capsule.

[a]Elimination half-life of the drug.

[b]Time to reach maximum plasma concentration.

[c]Maximum plasma concentration.

[d]Area under the concentration−time curve from 0 to 24 h.

[e]Mean residence time.

[f]DES−LMWH oral enteric capsule.

[g]$P < 0.05$ *vs.* C_{max} of Free LMWH (*p.o.*) group.

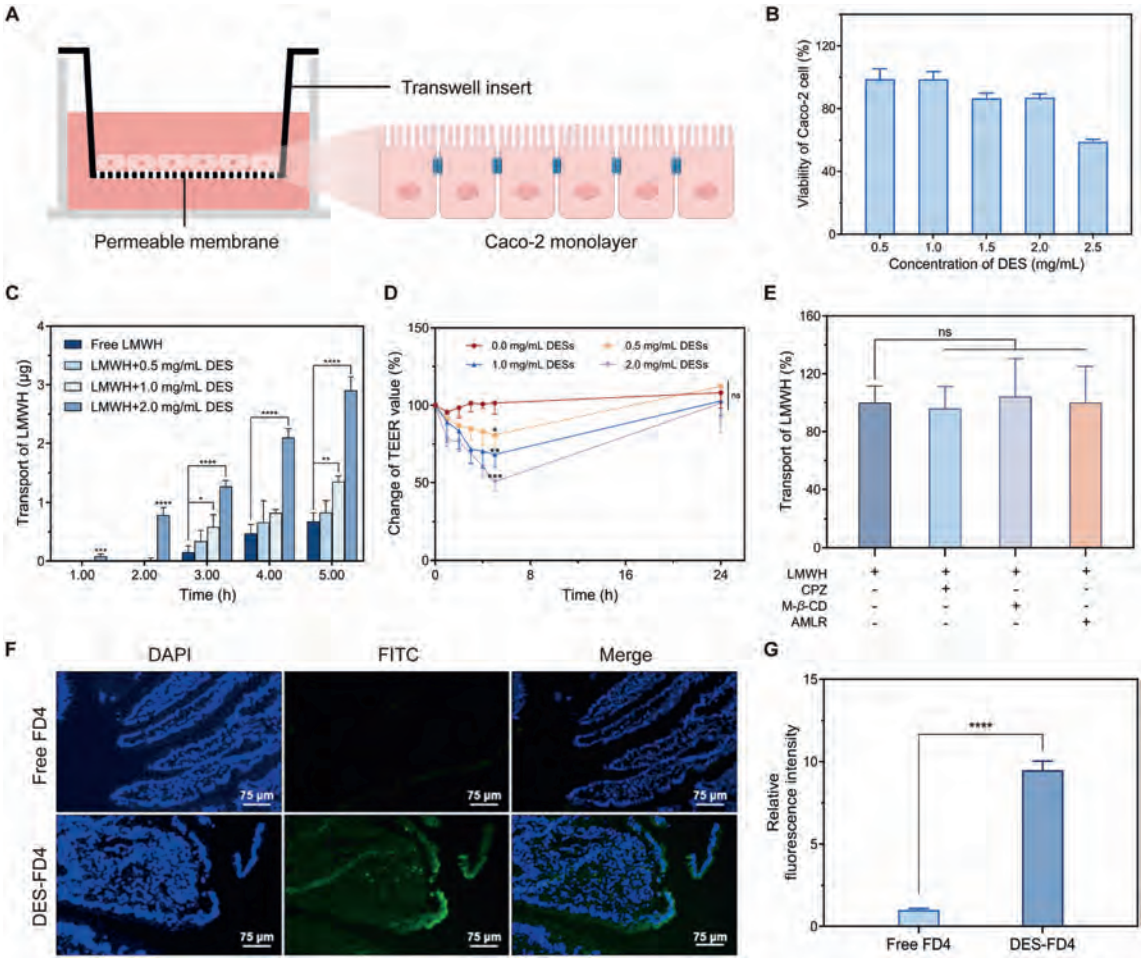

Figure 5 The mechanism by which DESs promote the intestinal absorption of LMWH. (A) The schematic illustration of the Caco-2 monolayer cell model. (B) The effect of DESs concentration on the activity of Caco-2 cells ($n = 6$). (C) The effect of DES concentration on the transport of LMWH. $^{*}P < 0.05$, $^{**}P < 0.01$, $^{***}P < 0.001$, $^{****}P < 0.0001$ *vs.* free LMWH group ($n = 3$). (D) The effect of DES concentration on TEER value. $^{*}P < 0.05$, $^{**}P < 0.01$, $^{***}P < 0.001$ *vs.* 0.0 mg/mL DESs group; ns, not significant ($n = 3$). (E) The effect of inhibitors on the transport of DES−LMWH. CPZ inhibits clathrin endocytosis by acting on intracellular dynein. M-β-CD inhibits caveolin endocytosis by regulating intracellular cholesterol levels and destroying actin required for transport. AMLR inhibits macropinocytosis by inhibiting Na^{+}/H^{+} exchange and lowering cell membrane pH ($n = 3$). (F) Penetration in the rat jejunal segments after *in vivo* intestinal perfusion and (G) semiquantitative analysis of fluorescence intensity. Blue and green fluorescence represent the nucleus and FD4. $^{****}P < 0.0001$ *vs.* free FD4 group ($n = 3$). Data are presented as mean ± SD. ns, not significant.

endocytosis pathways. The three inhibitors demonstrated little effect on DES−LMWH transport compared to the non-pretreated group (Fig. 5E). The results indicated that DESs did not alter LMWH transmembrane transport through the three major transcellular pathways: clathrin-mediated, caveolin-mediated, and micropinocytosis-mediated.

Finally, we investigated the intestinal penetration of DES formulation in the single-pass intestinal perfusion model using FD4 as a model molecule. As shown in Fig. 5F, free FD4 displayed modest green fluorescence in the intestinal tissue. In contrast, DESs significantly promoted the uptake of FD4 in the jejunal epithelial cell layer, primarily located in the apical columnar cell layer of the small intestinal villi and within the villi. The fluorescence intensity of the DES-FD4 group was approximately 9.48 times that of free FD4 (Fig. 5G). The results revealed that DESs potently promote the intestinal penetration of biological drugs.

3.6. Effects of in vivo thrombosis prophylaxis in $FeCl_3$-induced rat femoral venous thrombosis model

The effects of preparations preventing thrombosis were evaluated in $FeCl_3$-induced rat femoral venous thrombosis model (Fig. 6A and Supporting Information Fig. S6). Topical application of $FeCl_3$ to the femoral vein allowed Fe^{3+} to penetrate the vascular endothelium and generate reactive oxygen species (ROS) *via* the Fenton reaction, causing lipid peroxidation in endothelial cell membranes and endothelial injury[65]. The denuded vessels exposed subendothelial collagen, triggering platelet activation, adhesion and aggregation and forming primary platelet plugs. Meanwhile, the intrinsic blood coagulation cascade was initiated, transforming coagulation factor X to Xa, which led to thrombin production, catalyzing the cleavage of fibrinogen into fibrin monomers and ultimately forming a femoral venous thrombosis[66].

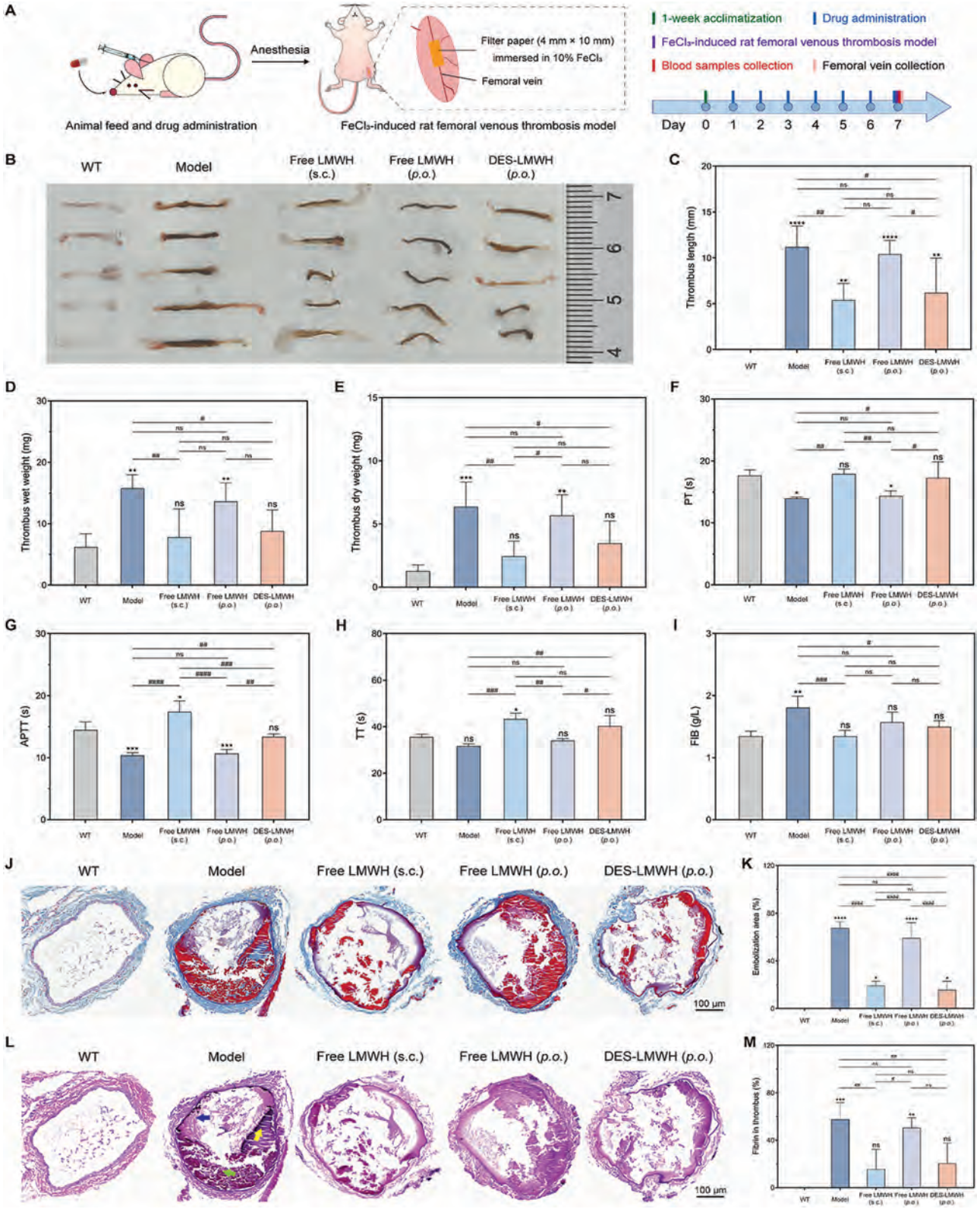

Figure 6 Effects of *in vivo* thrombosis prophylaxis in $FeCl_3$-induced rat femoral venous thrombosis model. (A) The rat femoral venous thrombosis model was induced by 10% $FeCl_3$ solution for 5 min. (B) The images of rat femoral venous thrombus. (C−E) The prophylactic effect of different treatments in thrombus length (C), thrombus wet-weight (D) and thrombus dry-weight (E). (F−I) Analysis of plasma coagulation parameters, including PT (F), APTT (G), TT (H), and FIB (I). (J, K) Analysis of femoral venous thrombus histopathology by Masson staining (J) and semiquantitative analysis of embolization area (K). Scale bar: 100 μm. (L, M) Analysis of femoral venous thrombus morphology by H&E staining (L) and semiquantitative analysis of fibrin proportion in thrombus (M). Blue arrow: fibrin; yellow arrow: platelets; green arrow: red blood cells. Scale bar: 100 μm. Data are presented as mean ± SD, $n = 5$. $^{*}P < 0.05$, $^{**}P < 0.01$, $^{***}P < 0.001$, $^{****}P < 0.0001$ *vs.* WT group; $^{\#}P < 0.05$, $^{\#\#}P < 0.01$, $^{\#\#\#}P < 0.001$, $^{\#\#\#\#}P < 0.0001$ *vs.* respective monotherapy group; ns, not significant.

As shown in Fig. 6B, the $FeCl_3$ induction resulted in obvious femoral venous thrombosis compared with the WT group, indicating successful establishment of the model. The size of the formed thrombus decreased in turn in the groups treated with LMWH (*p.o.*), DES−LMWH (*p.o.*), LMWH (s.c.) and the WT group compared with the model group. To quantify the thrombus alteration, we determined the thrombus length, wet weight and dry weight (Fig. 6C−E). The treatment using LMWH (*p.o.*) did not significantly decrease these indices. Whereas the DES−LMWH (*p.o.*) group demonstrated a significant reduction in the indexes and similar efficiency to the LMWH (s.c.) group. Then, we investigated the blood parameters, including prothrombin time (PT), activated partial thromboplastin time (APTT), thrombin time (TT) and fibrinogen (FIB) (Fig. 6F−I). The thrombus formation significantly decreased PT, APTT, and TT, while increasing FIB, indicating hypercoagulability, triggering the intrinsic coagulation pathway, and an increase in fibrinogen. While the treatment using LMWH (s.c.) or DES−LMWH (*p.o.*) combated the alterations. Finally, H&E staining and Masson staining of the embodied femoral veins were conducted to evaluate the thrombotic degree and the amount of crosslinked fibrin formation. As shown in Fig. 6J and K, venous endothelial injury and fibrosis were demonstrated in all $FeCl_3$-treated groups, and the vascular lumens of the model and LMWH (*p.o.*) groups were severely obstructed. By contrast, the embolization area in the LMWH (s.c.) and DES−LMWH (*p.o.*) groups decreased by 48.37% and 52.01%, respectively, compared with the model group, demonstrating similar efficacy. Moreover, the two treatments resulted in a 41.81% and 37.16% reduction in thrombus fibrin, respectively (Fig. 6L−M). Overall, the results indicated that DES−LMWH (*p.o.*) demonstrated similar efficacy to LMWH (s.c.) in preventing thrombosis formation, suggesting its potential to replace LMWH injection administration.

3.7. Safety evaluation

We evaluated the safety of DES−LMWH oral enteric capsules after repeated 7-day administration (Fig. 7A). The administration allowed little changes in the body weight (Fig. 7B) and little alteration in several toxicity indicators of liver and kidney (Fig. 7C−F), such as alanine aminotransferase (ALT), aspartate aminotransferase (AST), blood urea nitrogen (BUN) and creatinine (CR).

APTT is a commonly used clinical indicator that reflects the coagulation activity of the endogenous coagulation system and is widely used to assess the safety of heparin-based therapy. Meanwhile, PLT is also a factor that predicts the bleeding tendency[67,68]. As shown in Fig. 7 G and H, the two indicators remained unchanged after repeated administration compared with the saline group. The results indicated that orally dosing the capsule had a minimal tendency towards spontaneous bleeding. Moreover, the capsule administration demonstrated little alteration in intestine structure, such as the circular folds and boundaries, and showed no toxicity to the major organs compared to the saline group (Fig. 7I and J). Overall, these results suggested the biocompatibility of DES−LMWH oral enteric capsules.

4. Discussion

Despite LMWH being one of the preferred anticoagulants for VTE, pulmonary embolism (PE) and assisted reproduction, its clinical utility remains constrained by high molecular weight and negative surface charges. These inherent properties necessitate frequent injections, posing a critical barrier to patients' medication adherence. DESs synthesized by Ge and Ch exhibited excellent solubilization ability and skin permeability[33,48]. Inspired by the mechanisms of permeability-promoting DESs, the development of an oral formulation for LMWH using DESs@enteric technology represents a significant advancement in overcoming the inherent challenges of LMWH's poor oral bioavailability. By synthesizing DESs from Ge and choline Ch at an optimal molar ratio (2:1) and loading the DES−LMWH complex in enteric capsules, the optimal formulation achieved an absolute bioavailability of 19.93% in rats, a 1.9-fold increase over free LMWH, surpassing the threshold required for VTE prophylaxis. The results indicated that DESs were an effective intestinal permeation enhancer while providing a potential clinically viable alternative to injectable anticoagulants.

The significantly expanded bioavailability was attributed mechanistically to DES's ability to reversibly open the tight junctions between intestinal epithelial cells, thereby enhancing the efficiency of paracellular transport. This aligns with previous reports of DES-mediated oral insulin delivery[37]. However, our work diverged from conventional absorption enhancers (*e.g.*, surfactants or nanocarriers) by leveraging the dual functionality of DESs: (i) stabilizing LMWH against degradation and (ii) enhancing permeability without inducing cytotoxicity. Comparative analysis revealed a 4.3-fold greater intestinal permeability compared to free LMWH, highlighting the superiority of DESs in promoting intestinal permeability over traditional enhancers, such as chitosan derivatives[69]. For instance, Fan et al.[70] reported a 1.86-fold enhancement of intestinal permeability using LMWH with thiolated chitosan, which is lower than the 4.3-fold improvement achieved by DESs. Crucially, the reversibility of TEER reduction in Caco-2 monolayers (recovery >95% after DES removal) alleviated safety concerns associated with chronic tight junction disruption, a paramount consideration for extended anticoagulation regimens.

Compared to previously reported LMWH delivery systems, such as polymeric nanoparticle conjugates[22,71], a key improvement lies in the conversion of liquid DESs into stable solid granules *via* mannitol-assisted wet granulation, which enables scalable capsule production using conventional pharmaceutical manufacturing methods. The simplified manufacturing process (<5 excipients) coupled with enteric-capsule loading enabled the formulation to have long-term storage stability and low cost. Notably, the oral capsules demonstrated therapeutic equivalence to subcutaneous LMWH injections in prophylaxis. Moreover, the capsule has a duration of prophylactic plasma concentrations of more than 8 h (0.1−0.5 IU/mL) and a 7.5-h $t_{1/2}$ in blood. In contrast, LMWH (s.c.) demonstrates a 6-h duration and a 2.6-h $t_{1/2}$. The comparison indicated that the capsule could extend the action time and reduce the frequency of administration.

Venous thrombosis pathogenesis conforms to Virchow's triad, which includes endothelial injury, hypercoagulability and stasis[72,73]. Topical administration of $FeCl_3$ triggered oxidative damage to the vascular endothelium, exposed subendothelial collagen, initiated platelet adhesion and aggregation, activated the intrinsic coagulation cascade and resulted in hypercoagulability and fibrin formation. Then, the progressive thrombus formation trapped hemocytes and caused partial vascular occlusion, reducing blood flow velocity and resulting in stasis[72]. In this model, LMWH exerted antithrombotic effects by inhibiting factor Xa. At

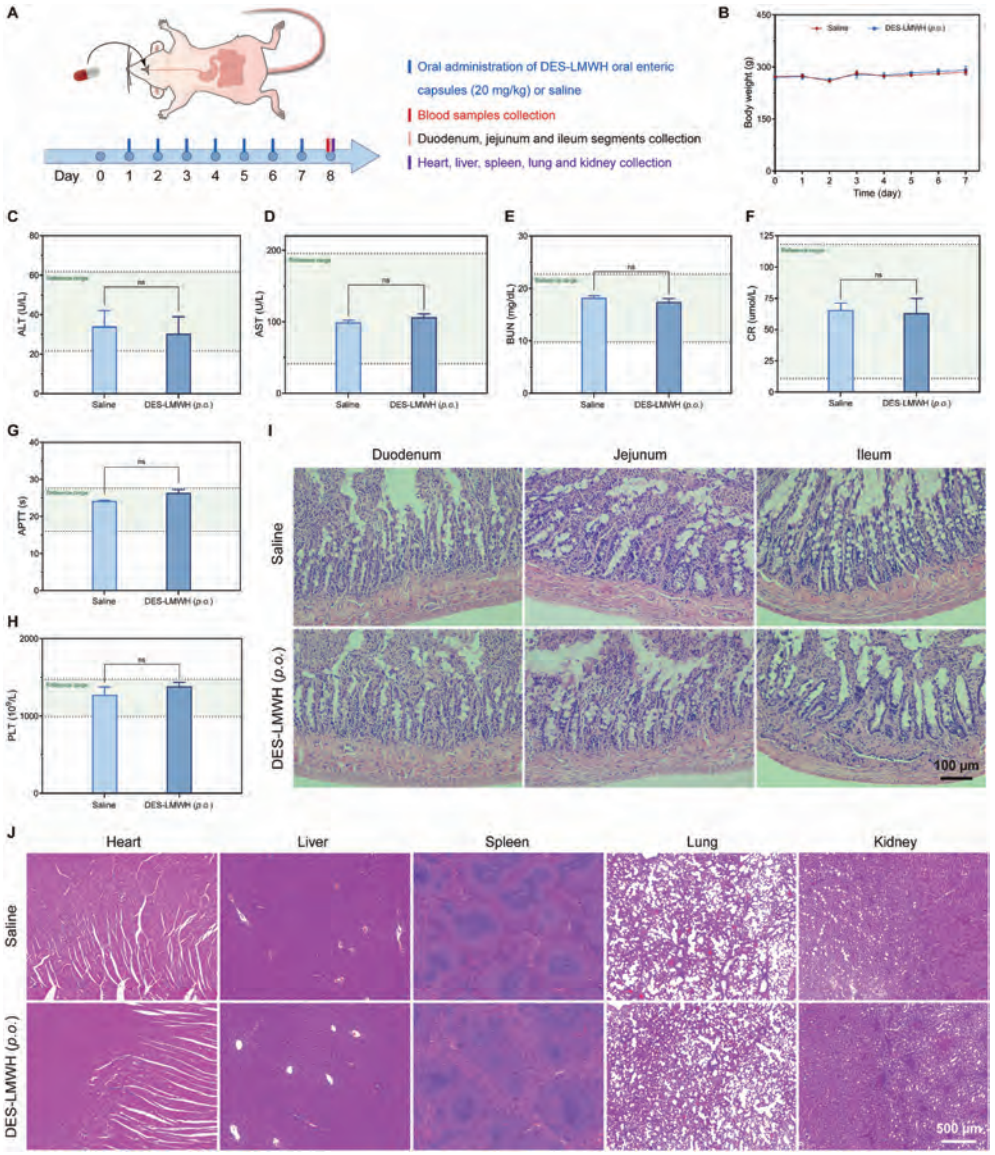

Figure 7 Safety evaluation of DES−LMWH oral enteric capsules. (A) Safety evaluation designs. Samples were collected after one week of continuous administration of saline and DES−LMWH oral enteric capsules. (B) Body weight changes in rats. (C−F) Assessment of liver and kidney function in rats using indicators including ALT (C), AST (D), BUN (E), and CR (F). (G) APTT activity of rat plasma. (H) Blood platelets. (I) H&E staining of rat intestine tissue sections. Scale bar: 100 μm. (J) H&E staining of major rat organs. Scale bar: 500 μm. Data are presented as mean ± SD, $n = 3$. ns, not significant.

prophylactic doses, it interrupted fibrin generation during the coagulation cascade. We therefore evaluated the antithrombotic efficacy of the formulation by quantifying the thrombus area and composition post-administration. The DES−LMWH oral enteric capsules and subcutaneous LMWH demonstrated significant thrombus reduction, decreasing by 52.01% and 48.37% in the embolization area, respectively. The results validated the antithrombotic activity of DES−LMWH oral enteric capsules and suggested potential clinical equivalence to subcutaneous LMWH.

Besides, several limitations warrant attention. The study utilized a rodent model to investigate bioavailability; however, intestinal tight junction proteins change both quantitatively and qualitatively in pigs, rats, and humans[74]. Validation in larger species should be conducted in the future to assess interspecies variability in DES-mediated absorption. Moreover, injectable LMWH undergoes renal clearance, whereas orally administered LMWH faces additional first-pass hepatic metabolism. This hepatic processing introduces potential liver toxicity concerns. Although preliminary safety evaluations indicate no drug-induced hepatorenal toxicity from the oral LMWH formulation, hepatic metabolism may preferentially degrade higher-molecular-weight LMWH components into smaller fragments. This theoretical size reduction could potentially enhance safety compared to injectable LMWH. However, detailed characterization of LMWH's metabolic fate during first-pass processing remains incomplete and needs further investigation. Additionally, patients who require anticoagulant therapy often have comorbidities of cardiovascular and cerebrovascular events, requiring the combined use of antihypertensive drugs, hypoglycemic drugs, etc., leading to the widespread phenomenon of polypharmacy[75-77]. The impact of DESs on the absorption of

concomitant medications remains unexplored, which is a critical consideration for patients with polypharmacy.

5. Conclusions

Our study presents a novel strategy for the effective oral delivery of LMWH, with great potential for clinical translation by transforming injectable LMWH into patient-friendly oral doses. This platform is promising to address critical adherence barriers in long-term anticoagulation therapy.

Acknowledgments

This study was supported by the National Natural Science Foundation of China (Nos. 82073782 and 82241002) and the Natural Science Foundation of Hebei Province (No. H2024206191, China).

Author contributions

Xiaoke He: writing − original draft, methodology, investigation, formal analysis, data curation. Jiahui Zou: methodology, investigation, formal analysis, data curation. Yuxin Jiang: methodology, investigation, formal analysis, data curation. Runrui Liao: methodology, formal analysis, data curation. Huiling Liao: methodology, formal analysis, data curation. Yaping Liu: methodology, formal analysis, data curation. Jing Yu: writing − review & editing. Yueming Zhao and Wei He: writing − review & editing, supervision, project administration, funding acquisition, formal analysis, data curation, conceptualization. All the authors have read and approved the final manuscript.

Conflicts of interest

The authors declare no conflicts of interest.

Appendix A. Supporting information

Supporting information to this article can be found online at https://doi.org/10.1016/j.apsb.2025.10.037.

References

1. Khan F, Tritschler T, Kahn SR, Rodger MA. Venous thromboembolism. *Lancet* 2021;**398**:64−77.
2. Middeldorp S, Nieuwlaat R, Baumann Kreuziger L, Coppens M, Houghton D, James AH, et al. American society of hematology 2023 guidelines for management of venous thromboembolism: thrombophilia testing. *Blood Adv* 2023;**7**:7101−38.
3. Ageno W. How we changed our approach to venous thromboembolism. *Haematologica* 2022;**107**:2286−7.
4. Betticher C, Bertaggia Calderara D, Matthey-Guirao E, Gomez FJ, Aliotta A, Lemmel E, et al. Global coagulation assays detect an early prothrombotic state in children with acute lymphoblastic leukemia. *J Thromb Haemost* 2024;**22**:2482−94.
5. Xie YY, Li XT, Wu JY, Zeng HL, Boucetta H, Wang BR, et al. CAR-T cells for cancer immunotherapy. *Chin Chem Lett* 2023;**34**:108202.
6. Guntupalli SR, Spinosa D, Wethington S, Eskander R, Khorana AA. Prevention of venous thromboembolism in patients with cancer. *BMJ* 2023;**381**:e072715.
7. Bistervels IM, Buchmüller A, Wiegers HMG, Ní Áinle F, Tardy B, Donnelly J, et al. Intermediate-dose versus low-dose low-molecular-weight heparin in pregnant and post-partum women with a history of venous thromboembolism (highlow study): an open-label, multicentre, randomised, controlled trial. *Lancet* 2022;**400**:1777−87.
8. Khorana AA, Mackman N, Falanga A, Pabinger I, Noble S, Ageno W, et al. Cancer-associated venous thromboembolism. *Nat Rev Dis Primers* 2022;**8**:11.
9. Schrag D, Uno H, Rosovsky R, Rutherford C, Sanfilippo K, Villano JL, et al. Direct oral anticoagulants *vs* low-molecular-weight heparin and recurrent VTE in patients with cancer: a randomized clinical trial. *JAMA* 2023;**329**:1924−33.
10. Frere C, Farge D, Schrag D, Prata PH, Connors JM. Direct oral anticoagulant *versus* low molecular weight heparin for the treatment of cancer-associated venous thromboembolism: 2022 updated systematic review and meta-analysis of randomized controlled trials. *J Hematol Oncol* 2022;**15**:69.
11. Yu YL, Song Y, Zhao YJ, Wang NN, Wei B, Linhardt RJ, et al. Quality control, safety assessment and preparation approaches of low molecular weight heparin. *Carbohydr Polym* 2024;**339**:122216.
12. Douketis JD, Spyropoulos AC, Murad MH, Arcelus JI, Dager WE, Dunn AS, et al. Perioperative management of antithrombotic therapy: an American college of chest physicians clinical practice guideline. *Chest* 2022;**162**:e207−43.
13. Gailani D, Gruber A. Targeting factor XI and factor XIa to prevent thrombosis. *Blood* 2024;**143**:1465−75.
14. Fang GH, Tang B. Advanced delivery strategies facilitating oral absorption of heparins. *Asian J Pharm Sci* 2020;**15**:449−60.
15. Zheng YX, Luo SQ, Xu M, He Q, Xie J, Wu JW, et al. Transepithelial transport of nanoparticles in oral drug delivery: from the perspective of surface and holistic property modulation. *Acta Pharm Sin B* 2024;**14**:3876−900.
16. Liu C, Liu W, Liu YH, Duan HX, Chen LQ, Zhang XT, et al. Versatile flexible micelles integrating mucosal penetration and intestinal targeting for effectively oral delivery of paclitaxel. *Acta Pharm Sin B* 2023;**13**:3425−43.
17. Lai YY, Xie B, Zhang WT, He W. Pure drug nanomedicines—Where we are?. *Chin J Nat Med* 2025;**23**:385−409.
18. Subedi L, Pandey P, Kang SH, Kim KT, Cho SS, Chang KY, et al. Enhanced oral absorption of teriparatide with therapeutic potential for management of osteoporosis. *J Control Release* 2022;**349**:502−19.
19. Xiao PF, Wang HX, Liu HB, Yuan HY, Guo C, Feng YP, et al. Milk exosome−liposome hybrid vesicles with self-adapting surface properties overcome the sequential absorption barriers for oral delivery of peptides. *ACS Nano* 2024;**18**:21091−111.
20. Motlekar NA, Srivenugopal KS, Wachtel MS, Youan BB. Modulation of gastrointestinal permeability of low-molecular-weight heparin by L-arginine: *in-vivo* and *in-vitro* evaluation. *J Pharm Pharmacol* 2006;**58**:591−8.
21. Hoffart V, Lamprecht A, Maincent P, Lecompte T, Vigneron C, Ubrich N. Oral bioavailability of a low molecular weight heparin using a polymeric delivery system. *J Control Release* 2006;**113**:38−42.
22. Al-Hilal TA, Park J, Alam F, Chung SW, Park JW, Kim K, et al. Oligomeric bile acid-mediated oral delivery of low molecular weight heparin. *J Control Release* 2014;**175**:17−24.
23. Wang LL, Sun YJ, Shi CJ, Li L, Guan J, Zhang X, et al. Uptake, transport and peroral absorption of fatty glyceride grafted chitosan copolymer−enoxaparin nanocomplexes: influence of glyceride chain length. *Acta Biomater* 2014;**10**:3675−85.
24. Bagre AP, Jain K, Jain NK. Alginate coated chitosan core shell nanoparticles for oral delivery of enoxaparin: *in vitro* and *in vivo* assessment. *Int J Pharm* 2013;**456**:31−40.
25. Yuan HY, Guo C, Liu L, Zhao LX, Zhang Y, Yin T, et al. Progress and prospects of polysaccharide-based nanocarriers for oral delivery of proteins/peptides. *Carbohydr Polym* 2023;**312**:120838.
26. Ghavami M, Pedersen J, Kjeldsen RB, Alstrup AKO, Zhang ZY, Koulianou V, et al. A self-unfolding proximity enabling device for oral delivery of macromolecules. *J Control Release* 2023;**361**:40−52.
27. Gao YY, Fan M, Cheng XX, Liu XF, Yang H, Ma WY, et al. Deep eutectic solvent: synthesis, classification, properties and application in macromolecular substances. *Int J Biol Macromol* 2024;**278**:134593.

28. Tian Y, Zhu MM, Hu TT, Liu CG. Natural deep eutectic solvent-a novel green solvent for protein stabilization. *Int J Biol Macromol* 2023;**247**:125477.
29. Xie B, Liu YP, Li XT, Yang P, He W. Solubilization techniques used for poorly water-soluble drugs. *Acta Pharm Sin B* 2024;**14**:4683−716.
30. Xu Y, Zhao M, Cao J, Fang T, Zhang J, Zhen Y, et al. Applications and recent advances in transdermal drug delivery systems for the treatment of rheumatoid arthritis. *Acta Pharm Sin B* 2023;**13**:4417−41.
31. Meyer LE, Andersen MB, Kara S. A deep eutectic solvent thermomorphic multiphasic system for biocatalytic applications. *Angew Chem Int Ed Engl* 2022;**61**:e202203823.
32. Huang WZ, Wu XY, Qi JP, Zhu QG, Wu W, Lu Y, et al. Ionic liquids: green and tailor-made solvents in drug delivery. *Drug Discov Today* 2020;**25**:901−8.
33. Xie B, Jiang Q, Zhu F, Lai YY, Zhao YM, He W, et al. Transdermal delivery of amphotericin B using deep eutectic solvents for antifungal therapy. *Chin Chem Lett* 2025;**36**:110508.
34. Wu XY, Yu Q, Wu J, Li T, Ding N, Wu W, et al. Ionic liquids containing ketoconazole improving topical treatment of T. *Interdigitale* infection by synergistic action. *Int J Pharm* 2020;**589**:119842.
35. Shi YJ, Zhao ZM, Gao YS, Pan DC, Salinas AK, Tanner EEL, et al. Oral delivery of sorafenib through spontaneous formation of ionic liquid nanocomplexes. *J Control Release* 2020;**322**:602−9.
36. Rogers RD, Gurau G. Is "choline and geranate" an ionic liquid or deep eutectic solvent system?. *Proc Natl Acad Sci U S A* 2018;**115**:E10999.
37. Banerjee A, Ibsen K, Brown T, Chen R, Agatemor C, Mitragotri S. Ionic liquids for oral insulin delivery. *Proc Natl Acad Sci U S A* 2018;**115**:7296−301.
38. Dharamdasani V, Mandal A, Qi QM, Suzuki I, Bentley M, Mitragotri S. Topical delivery of siRNA into skin using ionic liquids. *J Control Release* 2020;**323**:475−82.
39. Panse N, Gerk PM. The Caco-2 model: modifications and enhancements to improve efficiency and predictive performance. *Int J Pharm* 2022;**624**:122004.
40. Ogulur I, Pat Y, Aydin T, Yazici D, Rückert B, Peng YQ, et al. Gut epithelial barrier damage caused by dishwasher detergents and rinse aids. *J Allergy Clin Immunol* 2023;**151**:469−84.
41. Williams-Norwood T, Caswell M, Milner B, Vescera JC, Prymicz K, Ciszak AG, et al. Design and implementation of an anti-factor Xa heparin monitoring protocol. *AACN Adv Crit Care* 2020;**31**:129−37.
42. Milling Jr TJ, Middeldorp S, Xu L, Koch B, Demchuk A, Eikelboom JW, et al. Final study report of andexanet alfa for major bleeding with factor Xa inhibitors. *Circulation* 2023;**147**:1026−38.
43. Cheng CJ, Liu KX, Zhang JL, Han YQ, Zhang TJ, Hou YY, et al. Ginsenoside CK targets PHD2 to prevent platelet adhesion and enhance blood circulation by modifying the three-dimensional arrangement of collagen. *Acta Pharm Sin B* 2025;**15**:1497−513.
44. Peternel L, Drevensek G, Cerne M, Stalc A, Stegnar M, Budihna MV. Evaluation of two experimental venous thrombosis models in the rat. *Thromb Res* 2005;**115**:527−34.
45. Kudo D, Goto T, Uchimido R, Hayakawa M, Yamakawa K, Abe T, et al. Coagulation phenotypes in sepsis and effects of recombinant human thrombomodulin: an analysis of three multicentre observational studies. *Crit Care* 2021;**25**:114.
46. Moynihan KM, Johnson K, Rane M, Norman A, Humphreys S, Stocker C, et al. Pediatric thromboelastograph 6s and laboratory coagulation reference values. *Arch Pathol Lab Med* 2021;**145**:1413−23.
47. Tanner EEL, Ibsen KN, Mitragotri S. Transdermal insulin delivery using choline-based ionic liquids (CAGE). *J Control Release* 2018;**286**:137−44.
48. Liu YP, Wang D, Lai YY, Zou JH, Yang P, Wu ZF, et al. Deep eutectic solvents for essential-oil delivery and bacterial-infected wound healing. *Langmuir* 2024;**40**:23766−79.
49. Meng Y, Sui XY, Pan X, Zhang XY, Sui HM, Xu T, et al. Density-oriented deep eutectic solvent-based system for the selective separation of polysaccharides from astragalus membranaceus var. mongholicus under ultrasound-assisted conditions. *Ultrason Sonochem* 2023;**98**:106522.
50. Maretti E, Pavan B, Rustichelli C, Montanari M, Dalpiaz A, Iannuccelli V, et al. Chitosan/heparin polyelectrolyte complexes as ion-paring approach to encapsulate heparin in orally administrable SLN: *in vitro* evaluation. *Colloids Surf A Physicochem Eng Asp* 2021;**608**:125606.
51. Yan Y, Sun Y, Wang PC, Zhang R, Huo CC, Gao TT, et al. Mucoadhesive nanoparticles-based oral drug delivery systems enhance ameliorative effects of low molecular weight heparin on experimental colitis. *Carbohydr Polym* 2020;**246**:116660.
52. Chourasia VR, Bisht M, Pant KK, Henry RJ. Unveiling the potential of water as a co-solvent in microwave-assisted delignification of sugarcane bagasse using ternary deep eutectic solvents. *Bioresour Technol* 2022;**351**:127005.
53. Hong S, Li S, Meng X, Li P, Wang X, Su M, et al. Bile duct ligation differently regulates protein expressions of organic cation transporters in intestine, liver and kidney of rats through activation of farnesoid X receptor by cholate and bilirubin. *Acta Pharm Sin B* 2023;**13**:227−45.
54. Tang WW, Zhang YJ, Li P, Li B. Evaluation of intestinal drug absorption and interaction using quadruple single-pass intestinal perfusion coupled with mass spectrometry imaging. *Anal Chem* 2023;**95**:3218−27.
55. Yang H, Zhai BT, Fan Y, Wang J, Sun J, Shi YJ, et al. Intestinal absorption mechanisms of araloside A *in situ* single-pass intestinal perfusion and *in vitro* Caco-2 cell model. *Biomed Pharmacother* 2018;**106**:1563−9.
56. Berg S, Kärrberg L, Suljovic D, Seeliger F, Söderberg M, Perez-Alcazar M, et al. Impact of intestinal concentration and colloidal structure on the permeation-enhancing efficiency of sodium caprate in the rat. *Mol Pharm* 2022;**19**:200−12.
57. McCartney F, Jannin V, Chevrier S, Boulghobra H, Hristov DR, Ritter N, et al. Labrasol® is an efficacious intestinal permeation enhancer across rat intestine: *ex vivo* and *in vivo* rat studies. *J Control Release* 2019;**310**:115−26.
58. Wu H, Chen QY, Wang WZ, Chu S, Liu XX, Liu YJ, et al. Compound sophorae decoction enhances intestinal barrier function of dextran sodium sulfate induced colitis *via* regulating notch signaling pathway in mice. *Biomed Pharmacother* 2021;**133**:110937.
59. Hou S, Yu H, Liu C, Johnson AMF, Liu X, Jiang Q, et al. Intestinal epithelial cell NCoR deficiency ameliorates obesity and metabolic syndrome. *Acta Pharm Sin B* 2024;**14**:5267−85.
60. Kataoka M, Ohi Y, Sakanoue K, Minami K, Higashino H, Yamashita S. Impact of dietary intake of medium-chain triacylglycerides on the intestinal absorption of poorly permeable compounds. *Mol Pharm* 2020;**17**:212−8.
61. Li B, Jiao SW, Guo SQ, Xiao T, Zeng Y, Hu YW, et al. Deep eutectic solvent self-assembled reverse nanomicelles for transdermal delivery of sparingly soluble drugs. *J Nanobiotechnol* 2024;**22**:272.
62. Itoh S, Hiruta Y, Hashii N, Fujita N, Natsuga T, Hattori T, et al. Determination of galactosamine impurities in heparin sodium using fluorescent labeling and conventional high-performance liquid chromatography. *Biologicals* 2013;**41**:355−63.
63. Stevens SM, Woller SC, Baumann Kreuziger L, Doerschug K, Geersing GJ, Klok FA, et al. Antithrombotic therapy for VTE disease: compendium and review of chest gidelines 2012-2021. *Chest* 2024;**166**:388−404.
64. Geerts WH, Bergqvist D, Pineo GF, Heit JA, Samama CM, Lassen MR, et al. Prevention of venous thromboembolism: american college of chest physicians evidence-based clinical practice guidelines (8th edition). *Chest* 2008;**133**:381s−453s.
65. Tranter JD, Mikami RT, Kumar A, Brown G, Abd El-Aziz TM, Zhao YH, et al. LRRC8 complexes are ATP release channels regulating platelet activation and arterial thrombosis. *Blood* 2025;**146**:1110−26.
66. Mwiza JMN, Lee RH, Paul DS, Holle LA, Cooley BC, Nieswandt B, et al. Both G protein-coupled and immunoreceptor tyrosine-based activation motif receptors mediate venous thrombosis in mice. *Blood* 2022;**139**:3194−203.

67. Chornenki NLJ, Fralick M, Sholzberg M. International normalized ratio and activated partial thromboplastin time testing. *CMAJ* 2022; **194**:E1135.
68. Billoir P, Elie T, Levy JH, Besnier E, Dureuil B, Veber B, et al. Anticoagulation monitoring with activated partial thromboplastin time and anti-Xa activity in intensive care unit patients: interest of thrombin generation assay. *Int J Mol Sci* 2022;**23**:11219.
69. Li B, Xiao T, Guo SQ, Wu Y, Lai RR, Liu ZY, et al. Oxymatrine-fatty acid deep eutectic solvents as novel penetration enhancers for transdermal drug delivery: formation mechanism and enhancing effect. *Int J Pharm* 2023;**637**:122880.
70. Fan B, Xing Y, Zheng Y, Sun C, Liang GX. pH-responsive thiolated chitosan nanoparticles for oral low-molecular weight heparin delivery: *in vitro* and *in vivo* evaluation. *Drug Deliv* 2016;**23**:238−47.
71. Huang L, Hu W, Huang LQ, Zhou QX, Song ZY, Tao HY, et al. "Two-birds-one-stone" oral nanotherapeutic designed to target intestinal integrins and regulate redox homeostasis for UC treatment. *Sci Adv* 2024;**10**:eado7438.
72. Camaj A, Fuster V, Giustino G, Bienstock SW, Sternheim D, Mehran R, et al. Left ventricular thrombus following acute myocardial infarction: JACC state-of-the-art Review. *J Am Coll Cardiol* 2022;**79**: 1010−22.
73. Zhao YC, Wang ZH, Zhao HM, Yap NA, Wang R, Cheng WL, et al. Sensing the future of thrombosis management: integrating vessel-on-a-chip models, advanced biosensors, and AI-driven digital twins. *ACS Sens* 2025;**10**:1507−20.
74. Søfteland JM, Casselbrant A, Biglarnia AR, Linders J, Hellström M, Pesce A, et al. Intestinal preservation injury: a comparison between rat, porcine and human intestines. *Int J Mol Sci* 2019;**20**:3135.
75. Volgman AS, Nair G, Lyubarova R, Merchant FM, Mason P, Curtis AB, et al. Management of atrial fibrillation in patients 75 years and older: JACC state-of-the-art review. *J Am Coll Cardiol* 2022;**79**:166−79.
76. Shantsila E, Choi EK, Lane DA, Joung B, Lip GYH. Atrial fibrillation: comorbidities, lifestyle, and patient factors. *Lancet Reg Health Eur* 2024;**37**:100784.
77. Marie S, Frost KL, Hau RK, Martinez-Guerrero L, Izu JM, Myers CM, et al. Predicting disruptions to drug pharmacokinetics and the risk of adverse drug reactions in non-alcoholic steatohepatitis patients. *Acta Pharm Sin B* 2023;**13**:1−28.